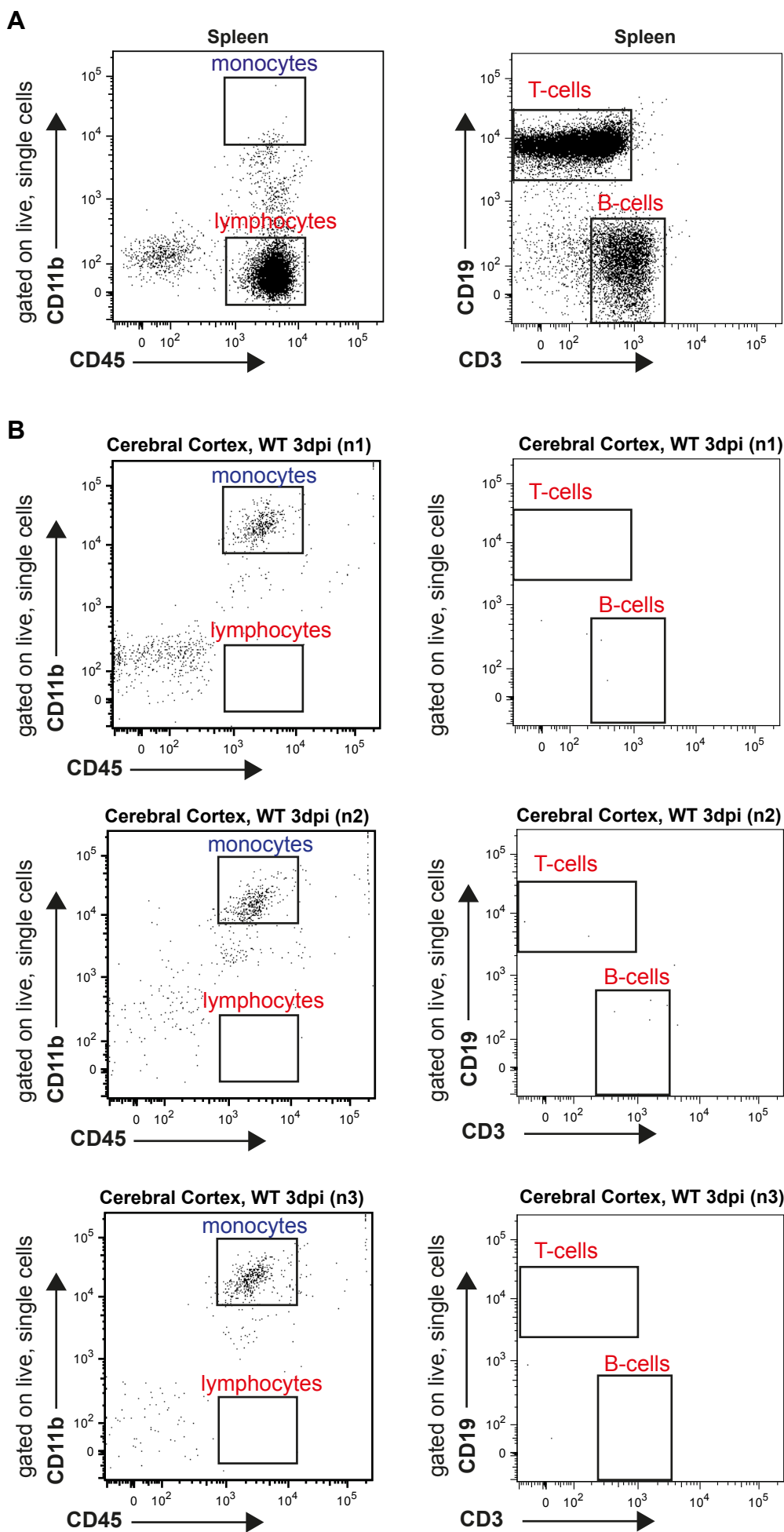
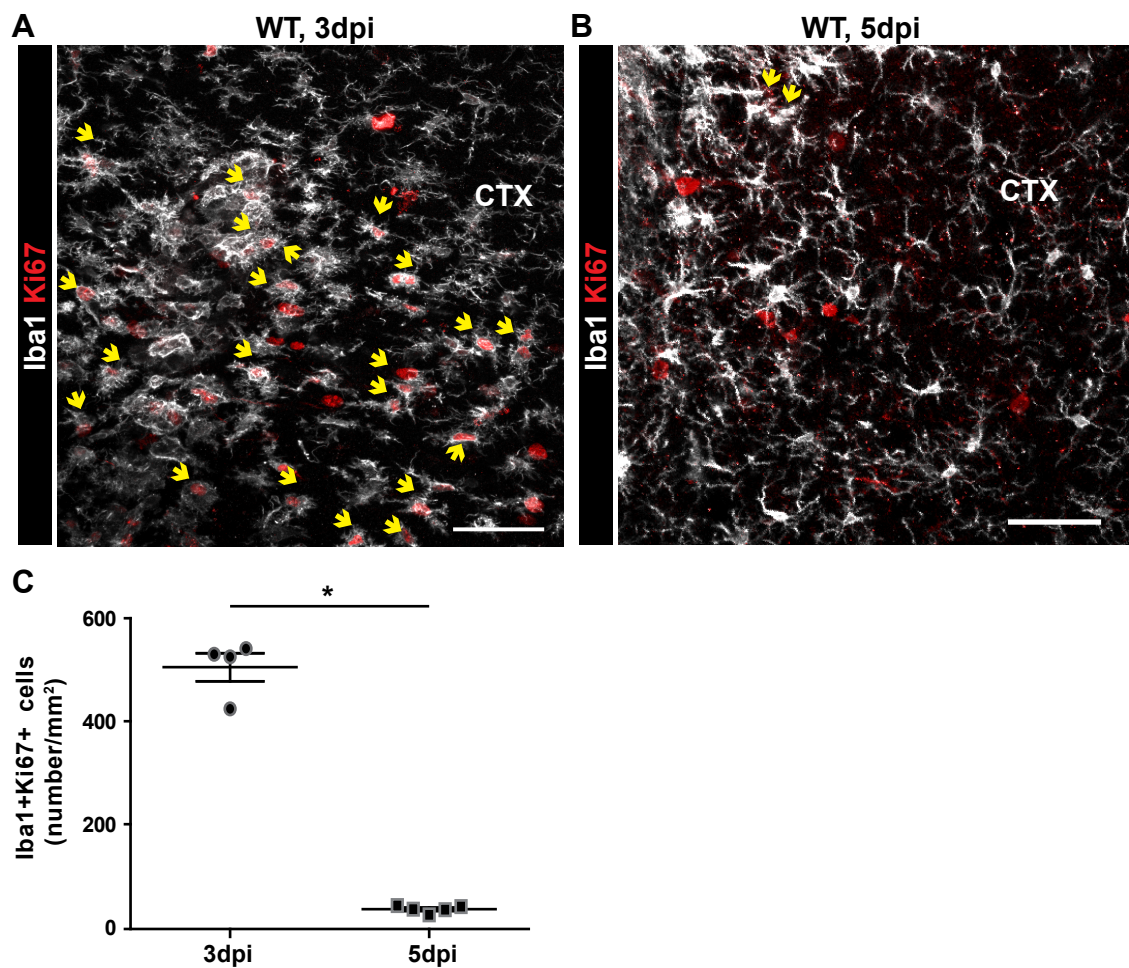


TABLE OF CONTENT

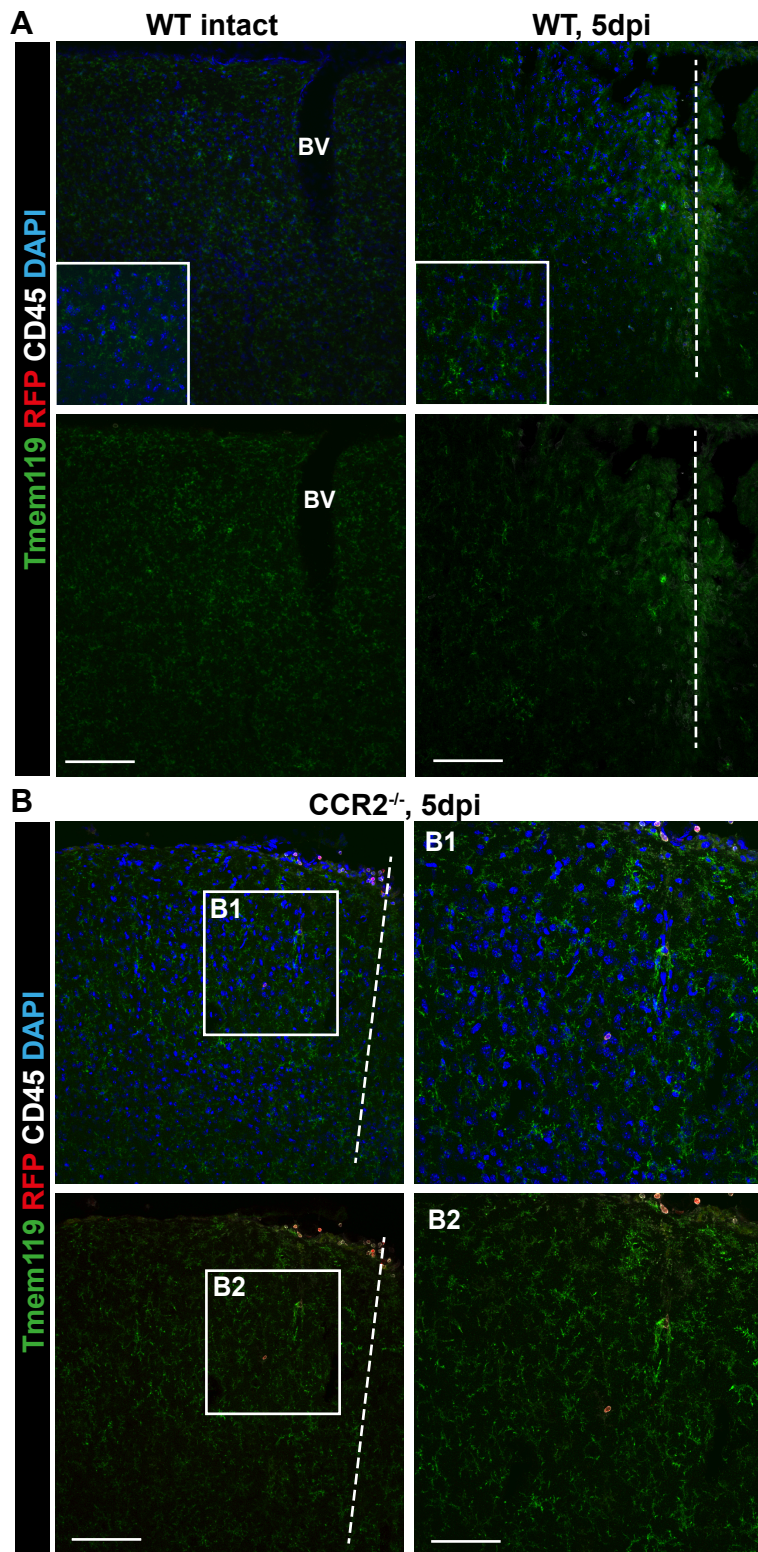
Appendix Figure S1. Absence of lymphocytes and predominance of CD45+/CD11b+ CD45+/CD11b+ monocytes/macrophages in the injured GM parenchyma at 3dpi	1
Appendix Figure S2. Microglia proliferation between 3 and 5 days after injury	2
Appendix Figure S3. Tmem119+ microglia around the stab- wound injury site of WT and CCR2 ^{-/-} mice at 5dpi	3
Appendix Figure S4. Faster resealing of the Blood-Brain Barrier (BBB) in the absence of monocyte invasion	4
Appendix Figure S5. Collagen I immunostaining in WT and CCR2 ^{-/-} mice at 28dpi	5
Appendix Figure S6. Reduced astrogliotic scar in CCR2 ^{-/-} mice at 90dpi	6
Appendix Figure Legends	7-9
Appendix Table S1. Significantly regulated proteins in the biopsy of the injury site isolated at 5dpi from WT compared to CCR2 ^{-/-} mice	10
Appendix Table S2. Biological processes overrepresented with proteins more abundant in WT	11
Appendix Table S3. Biological processes overrepresented with proteins more abundant in CCR2	12
Appendix Table S4. Primary and secondary antibodies used for immunohistological analysis	13



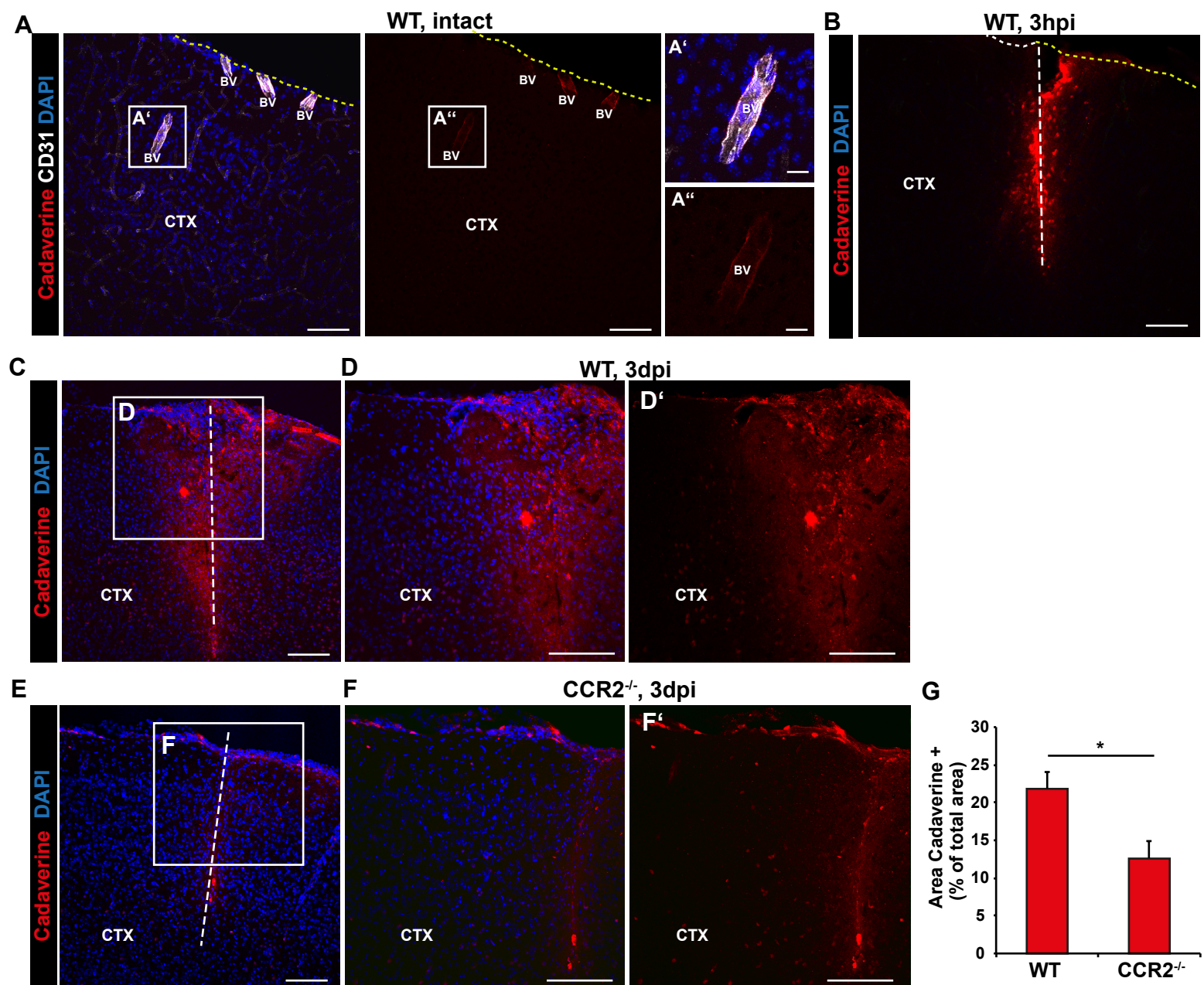
Appendix Figure S1



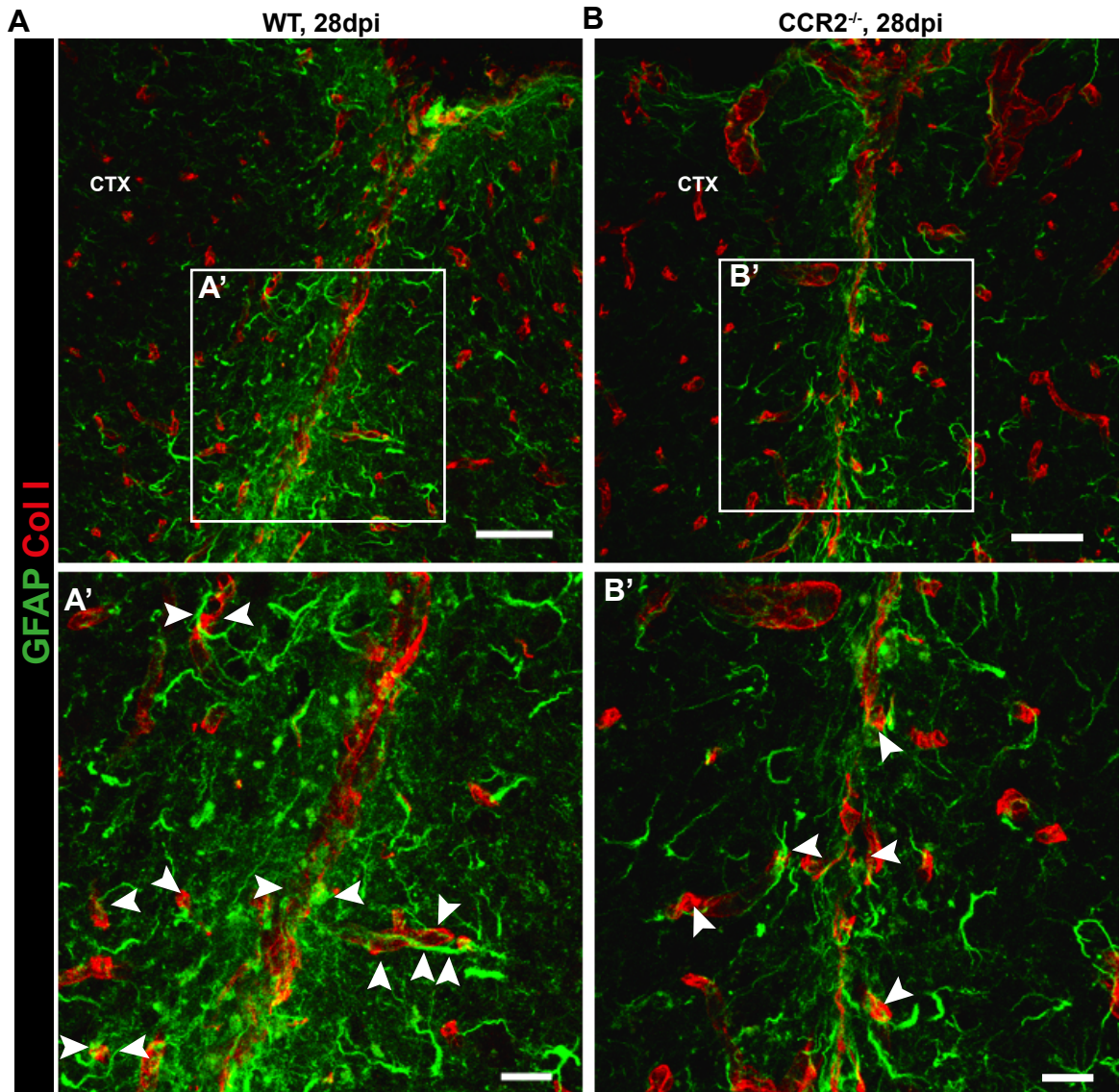
Appendix Figure S2



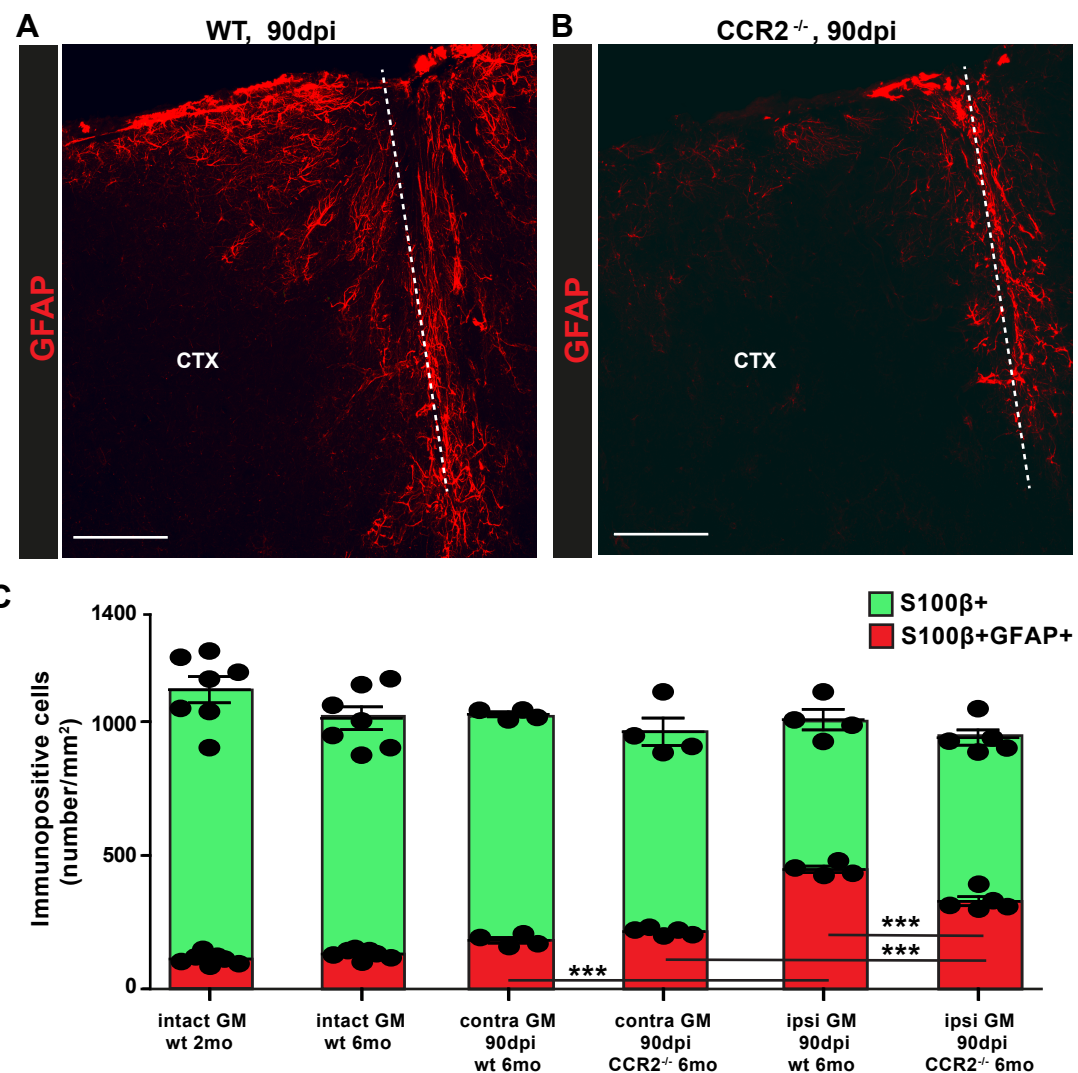
Appendix Figure S3



Appendix Figure S4



Appendix Figure S5



Appendix Figure S6

Appendix Figure Legends

Appendix Figure S1: Absence of lymphocytes and predominance of CD45⁺/CD11b⁺ monocytes/macrophages in the injured GM parenchyma at 3 dpi.

Fluorescence-Activated Cell Sorting (FACS) of CD45⁺ cells (isolated previously by magnetic activated cell sorting) was performed on spleen (**A**) and CD45⁺ cells from the GM tissue at 3dpi isolated by MACS (**B**). The identity of CD45⁺ cells was determined by staining with CD11b (high: monocytes/macrophages, see B, n1, left panel; low: lymphocytes, see A), CD19 (T-cells, see A, right panel) and CD3 (B-cells, see A right panel). While lymphocytes were readily detectable in samples taken from spleen (**A**), they were absent in brain tissue collected from the lesion site where CD45⁺ cells were exclusively CD11b high monocytes/macrophages.

Appendix Figure S2: Microglia proliferation between 3 and 5 days after injury.

Confocal images of Iba1 and Ki67 double-immunostaining in WT GM at 3 dpi (**A**) and 5 dpi (**B**). Arrows point to double-positive cells, the proliferating microglia at the injury site. (**C**) Histogram depicting the number of Iba1⁺Ki67⁺ cells in the injured cortical GM of WT mice at 3 dpi and 5 dpi. Of note, there was the steep decline in microglia proliferation at the injury site between 3-5 dpi. Data are represented as mean \pm SEM per independent experiments ($p=0.0159$, $n=4$ for 3 dpi and $n=5$ for 5 dpi). Marks represent individual data points. Significance of differences between means was analyzed using Mann-Whitney test. Scale bars: 50 μ m.

Appendix Figure S3: Tmem119+ microglia around the stab-wound injury site of WT and CCR2^{-/-} mice at 5 dpi. Representative confocal images of Tmem119 immunostaining in the intact (left panel) or injured (right panel) GM of WT (**A**) or CCR2^{-/-} mice (**B**) shown with DAPI staining to visualize nuclei in the upper row and without DAPI in the lower row of panels. Higher magnification views are shown as boxes in (**A**) and as separate panels in B1 and B2 (location is indicated by boxed area in the left panels of B). The dashed lines indicate the injury site. Note the increase in Tmem119 immunostaining at the lesion site. Scale bars: 125µm (A, B), 50µm (B1, B2).

Appendix Figure S4: Faster resealing of the Blood-Brain Barrier (BBB) in the absence of monocyte invasion. Confocal images of the intact GM parenchyma showing restriction of 1-kDa Alexa Fluor 555–Cadaverine exclusively to the cerebral vasculature (**A**). Higher magnification view of the boxed areas (**A'** and **A''** in **A**) shows Cadaverine within the lumen of blood vessels (BV). Representative images displaying the injury-related extravasation of Cadaverine-Alexa-555 into the GM parenchyma at 3 hours (3hpi) (**B**) and 3 days post stab wound in WT (**C, D**) and CCR2^{-/-} (**E, F**) mice. The dashed lines indicate the site of injury. The cell nuclei were counterstained with DAPI and this staining is omitted in the panels **D'** and **F'**. (**G**) Quantification of Cadaverine labelled area within the injured GM at 3 dpi showed a significant reduction in in CCR2^{-/-} stab wound injured brains (Mann-Whitney test, * $p=0.0376$, n=6), suggesting faster resealing of the BBB in the absence of monocyte invasion. Data are represented as mean ± SEM per independent experiments. Scale bars: 100µm (A, B, C, D), 30µm (A', A'').

Appendix Figure S5: Collagen I immunostaining in WT and CCR2^{-/-} mice at 28 dpi.

Representative confocal images showing Collagen 1- and GFAP-immunoreactivity at the injury site in WT (**A**) and CCR2^{-/-} (**B**) mice at 28dpi. Higher magnification view of the boxed areas (**A'** in **A**, and **B'** in **B**) showing reduction in collagen I deposits in the center of the lesion (center of boxed areas) and fewer GFAP reactive cells and processes (arrowheads) at the collagen1⁺ structures around the injury site in the CCR2^{-/-} compared to WT mice. Scale bars: 100μm (A, B).

Appendix Figure S6: Reduced astrogliotic scar in CCR2^{-/-} mice at 90 dpi. Confocal images displaying GFAP in the injured GM from WT (**A**) and CCR2^{-/-} (**B**) mice at 90dpi. Histogram in (**C**) depicts the total number of astrocytes (S100 β +), reactive (GFAP+ and S100 β +) and GFAP+ cells in a comparable region of the cerebral cortex GM at the injury site (ipsilateral) or in the contralateral hemisphere. Note that the increased astrocyte proliferation in CCR2^{-/-} mice does not lead to a permanent increase in astrocyte numbers and rather results in a significant reduction of GFAP+ cells at 90 dpi. All data are represented as mean ± SEM per independent experiments (n=7 for intact 6 months old WT mice, n=4 for WT 90 dpi and n=5 for CCR2 KO mice). Marks depict individual data points (animals). Significance of differences between means was analyzed using one way ANOVA with Tukeys post-hoc test and is indicated based on the *p* value (***p*<0.0001). Scale bars: 125μm.

Table S1
Significantly different proteins in the injured hemisphere of WT mice compared to injured CCR2^{-/-}

Table S2

Biological processes overrepresented with proteins more abundant in WT							List of observed genes	
Biological processes (GO-Term)		GO-Term ID	P-value	Fold enrichment	# Genes (observed)	# Genes (expected)	# Genes (total)	
one-carbon compound transport	one-carbon compound metabolism	GO_0019755	0.0001	175.0	2	0.0	14	Slc14at, Car12
mucopolysaccharide metabolism process	GO_0036510	0.0010	43.0	2	0.0	57	Ihh3, B3galact2	
uterine smooth muscle cell differentiation	GO_0019759	0.0015	612.5	1	0.0	5	Tshz2	
immunoglobulin biosynthetic process	GO_0002022	0.0022	28.8	2	0.1	85	Tshz3, B3galact2	
kidney smooth muscle tissue development	GO_0072194	0.0024	408.4	1	0.0	3	Tshz3	
negative regulation of isotype switching to IgE isotypes	GO_0048294	0.0024	408.4	1	0.0	3	Ntfip1	
aminoacyl transferase process	GO_0009502	0.0028	24.8	2	0.1	99	Ihh3, B3galact2	
regulation of cell cycle	GO_0009503	0.0028	306.3	1	0.0	3	Tshz3	
negative regulation of isotype switching	GO_0048295	0.0033	306.3	1	0.0	4	Ntfip1	
urea transmembrane transport	GO_0017918	0.0041	245.0	1	0.0	5	Slc14at	
uterine smooth muscle cell differentiation	GO_0027213	0.0041	245.0	1	0.0	5	Tshz3	
greater smooth muscle development	GO_0027214	0.0041	245.0	1	0.0	5	Tshz3	
intermediate filament bundle assembly	GO_0015165	0.0043	245.0	1	0.0	5	Cars3	
urea transport	GO_0015840	0.0043	245.0	1	0.0	6	Krt14	
isotype switching to IgE isotypes	GO_0048289	0.0057	175.0	1	0.0	6	Slc14at	
regulation of cell cycle, G1/S transition, S production	GO_0009504	0.0057	175.0	1	0.0	7	Ntfip1	
regulation of isotype switching to IgE isotypes	GO_0048293	0.0057	175.0	1	0.0	7	Ntfip1	
mRNA loading onto RISC involved in gene silencing by miRNA	GO_0035280	0.0057	175.0	1	0.0	7	Apo4	
negative regulation of B cell mediated immunity	GO_0002713	0.0065	153.1	1	0.0	8	Ntfip1	
negative regulation of immunoglobulin mediated immune response	GO_0002714	0.0065	153.1	1	0.0	8	Ntfip1	
small RNA loading onto RISC	GO_0070922	0.0065	153.1	1	0.0	8	Ano4	
carbon dioxide transport	GO_0015670	0.0068	153.1	1	0.0	8	Cart12	
negative regulation of autophagosome assembly	GO_1902902	0.0073	136.1	1	0.0	9	Fez2	
chloride ion homeostasis	GO_0009505	0.0081	122.5	1	0.0	10	Cart12	
negative regulation of immunoglobulin production	GO_0002638	0.0081	122.5	1	0.0	10	Ntfip1	
SRP-dependent cotranslational protein targeting to membrane	GO_0006614	0.0089	111.4	1	0.0	11	Sar3	
positive regulation of smooth muscle cell differentiation	GO_0051152	0.0089	111.4	1	0.0	11	Tshz3	
positive regulation of smooth muscle cell differentiation	GO_0051153	0.0089	111.4	1	0.0	11	Cart12	
negative regulation of type I immune response	GO_0028289	0.0089	111.4	1	0.0	11	Ntfip1	
regulation of isotype switching to IgG isotypes	GO_0048302	0.0098	102.1	1	0.0	12	Ntfip1	
adenylate cyclase-activating dopamine receptor signaling pathway	GO_0007191	0.0098	102.1	1	0.0	12	Gnai1	
smooth muscle contraction	GO_0009506	0.0102	102.1	1	0.0	12	Gnai3	
Fluid transport	GO_0020857	0.0106	94.2	1	0.0	13	Tshz3	
isotype switching to IgG isotypes	GO_0048291	0.0106	94.2	1	0.0	13	Ntfip1	
transport	GO_006810	0.0108	2.4	8	3.3	4087	Bln2, Slc14at, Fez1, Tmem63c, Cep83, Sar3, Ntfip1, Cart12	
crosselle assembly	GO_0007125	0.0125	67.5	3	0.0	579	Bln2, Fez1, Cep83	
membrane tubulation	GO_0027131	0.0144	87.5	1	0.0	14	Cart12	
establishment of mitochondrial localization	GO_0005164	0.0144	87.5	1	0.0	14	Fez1	
pre-mRNA processing	GO_0031064	0.0144	87.5	1	0.0	14	Apo4	
pre-mRNA processing	GO_0031065	0.0144	87.5	1	0.0	14	Apo4	
miRNA mediated inhibition of translation	GO_0035278	0.0122	81.7	1	0.0	15	Apo4	
cotranslational protein targeting to membrane	GO_0006613	0.0122	81.7	1	0.0	15	Sar3	
ubiquitin-dependent protein catabolic process via the multicellular body sorting pathway	GO_0043162	0.0122	81.7	1	0.0	15	Ntfip1	
regulation of translation, ncRNA-mediated	GO_0009507	0.0124	78.5	1	0.0	16	Cart12	
negative regulation of translation, ncRNA-mediated	GO_0040033	0.0130	76.6	1	0.0	16	Apo4	
gas transport	GO_0015669	0.0130	76.6	1	0.0	16	Cart12	
establishment of localization	GO_0051234	0.0133	2.3	8	0.5	4232	Bln2, Slc14at, Fez1, Tmem63c, Cep83, Sar3, Ntfip1, Cart12	
negative regulation, biotinidase biosynthetic process	GO_0009514	0.0133	2.3	7.1	0.0	21	Bln2	
activation of adenylate cyclase activity	GO_0006833	0.0138	72.1	1	0.0	17	Slc14at	
protein targeting to ER	GO_0045047	0.0146	68.1	1	0.0	18	Sar3	
negative regulation of autophagy	GO_0009515	0.0170	58.3	1	0.0	21	Tshz3	
negative regulation of organelle assembly	GO_0009516	0.0170	58.3	1	0.0	21	Fez1	
negative regulation of organelle localization to endoplasmic reticulum	GO_1902116	0.0178	55.7	1	0.0	22	Fez1	
centrosome localization	GO_0051642	0.0178	55.7	1	0.0	22	Cep83	
negative regulation of DNA recombination	GO_0045910	0.0178	55.7	1	0.0	22	Ntfip1	
regulation of respiratory caspase exchange	GO_0043576	0.0186	53.3	1	0.0	23	Tshz3	
negative regulation of metabolic process	GO_0040406	0.0190	53.3	1	0.0	24	Bln2	
fluid transport	GO_0042044	0.0194	51.0	1	0.0	24	Slc14at	
intermediate filament organization	GO_0045109	0.0194	51.0	1	0.0	24	Krt14	
negative regulation of macroautophagy	GO_0016242	0.0194	51.0	1	0.0	24	Fez1	
translational elongation	GO_0070193	0.0194	51.0	1	0.0	24	Apo4	
negative regulation of process	GO_0009517	0.0194	51.0	1	0.0	25	Bln2	
positive regulation of organelle localization	GO_0009518	0.0194	51.0	1	0.0	26	Ntfip1	
negative regulation of type II immune response	GO_0028288	0.0210	47.1	1	0.0	26	Cart12	
ion homeostasis	GO_0055081	0.0210	47.1	1	0.0	27	Tshz3	
smooth muscle tissue development	GO_0048745	0.0218	45.4	1	0.0	28	Bln2	
regulation of activity	GO_0009519	0.0218	43.8	1	0.0	28	B3galact2	
chondroitin sulphate carbohydrate metabolic process,	GO_0056554	0.0226	43.8	1	0.0	28	Apo4	
production of miRNAs involved in gene silencing by miRNA	GO_0035196	0.0226	43.8	1	0.0	28	Bln2	
regulation of interleukin-4 production	GO_0032673	0.0234	42.2	1	0.0	29	Ntfip1	
negative regulation of production of molecular mediator of immune response	GO_0009524	0.0234	42.2	1	0.0	29	Ntfip1	
synthesis of small RNA involved in gene silencing by RNA	GO_0070918	0.0234	42.2	1	0.0	29	Apo4	
dsRNA fragmentation	GO_0031050	0.0234	42.2	1	0.0	29	Apo4	
positive regulation of organelle localization	GO_0045762	0.0242	40.8	1	0.0	30	Gnai1	
protein localization to endoplasmic reticulum	GO_0009520	0.0250	39.5	1	0.0	31	Cep83	
broken localization to cytoskeleton	GO_0026288	0.0250	39.5	1	0.0	31	Ntfip1	
dopamine receptor signaling pathway	GO_0070712	0.0250	39.5	1	0.0	31	Fez1	
interleukin-4 production	GO_0032633	0.0250	34.0	1	0.0	36	Ntfip1	
negative regulation of cell cycle	GO_0009525	0.0250	32.9	2	1.8	2175	Apo4, Tie6, Fer1, Tshz3, Ntfip1	
establishment of organelle localization	GO_0051656	0.0304	7.3	2	0.3	337	Fez1, Cep83	
positive regulation of lysase activity	GO_0051349	0.0306	32.2	1	0.0	38	Gnai1	
protein localization to endolysosomal reticulum	GO_0070972	0.0306	32.2	1	0.0	38	Sar3	
negative regulation of lymphocyte mediated immunity	GO_0009526	0.0306	32.2	1	0.0	38	Ntfip1	
cellular iron homeostasis	GO_0009527	0.0306	32.2	1	0.0	38	Tshz3	
cell differentiation involved in kidney development	GO_0081005	0.0306	32.2	1	0.0	38	Gnai1	
positive regulation of cyclase activity	GO_0031281	0.0306	32.2	1	0.0	38	Apo4	
male meiosis	GO_0009528	0.0314	31.4	1	0.0	39	Bln2	
regulation of vacuole organization	GO_0009529	0.0314	31.4	1	0.0	39	Cart12	
multicellular organism movement	GO_0050879	0.0361	27.2	1	0.0	45	Tshz3	
RNA secondary structure unwinding	GO_0010501	0.0361	27.2	1	0.0	45	Apo4	
cellular response to GRIN1 ligand	GO_0071359	0.0361	27.2	1	0.0	45	Bln2	
positive regulation of process	GO_0009530	0.0361	27.2	1	0.0	45	Cart12	
cellular developmental process	GO_0048869	0.0363	2.1	7	3.3	4089	Krt14, Apo4, Tie6, Fer1, Tshz3, Cep83, Ntfip1	
positive regulation of cell differentiation	GO_0045957	0.0370	4.0	3	0.7	918	Tie6, Fer1, Tshz3	
glycosaminoglycan biosynthetic process	GO_0009624	0.0377	26.1	1	0.0	47	B3galact2	
regulation of cyclase activity	GO_0045761	0.0385	25.5	1	0.0	48	Cart12	
negative regulation of leukocyte mediated immunity	GO_0027074	0.0385	25.5	1	0.0	48	Ntfip1	
somatic recombination of immunoglobulin genes involved in immune response	GO_0022044	0.0385	25.5	1	0.0	48	Bln2	
somatic recombination of immunoglobulin genes involved in immune response	GO_0022038	0.0385	25.5	1	0.0	48	Cart12	
regulation of cell differentiation	GO_0009535	0.0393	3.0	4	1.3	1624	Tie6, Fer1, Tshz3, Ntfip1	
regulation of cell differentiation	GO_0031114	0.0393	2.9	3	0.8	1741	Tie6, Fer1, Tshz3, Ntfip1	
immunoglobulin production involved in immunoglobulin mediated immune response	GO_0023811	0.0400	24.5	1	0.0	50	Ntfip1	
regulation of biological process	GO_0060233	0.0408	24.0	1	0.0	51	B3galact2	
regulation of immunoglobulin mediated immune response	GO_0044045	0.0412	23	5	2.0	2430	Krt14, Bln2, Apo4, Fez1, Cep83	
regulation of biological process	GO_0044046	0.0412	23	5	2.0	2430	Krt14, Bln2, Apo4, Fez1, Cep83	
regulation of autophagy	GO_0048278	0.0416	23.6	1	0.0	52	Cep83	
regulation of B cell mediated immunity	GO_0010507	0.0416	23.6	1	0.0	52	Fez1	
homologous chromosome segregation	GO_0027122	0.0416	23.6	1	0.0	52	Ntfip1	
cellular response to receptor activity	GO_0032410	0.0424	23.1	1	0.0	53	Ntfip1	
smoltic differentiation of immunoglobulins	GO_0016445	0.0432	22.7	1	0.0	54	Ntfip1	
respiratory gaseous exchange	GO_0079585	0.0432	22.7	1	0.0	54	Tshz3	
regulation of immunoglobulin production	GO_0051640	0.0434	6.0	2	0.3	410	Fez1, Cep83	
regulation of cyclase activity	GO_0031279	0.0435	2.9	1	0.0	55	Ntfip1	
phagocytosis engulfment	GO_0068111	0.0443	21.5	1	0.0	57	Gnai1	
chromosome organization involved in meiotic cell cycle	GO_0070912	0.0443	21.5	1	0.0	58	Bln2	
cellular differentiation of immune receptors via germline recombination within a single locus	GO_0016444	0.0463	21.1	1	0.0	58	Apo4	
regulation of nucleic acid recombination	GO_0051339	0.0471	20.8	1	0.0	58	Ntfip1	
regulation of T cell proliferation	GO_0042130	0.0471	20.8	1	0.0	59	Gnai1	
localization	GO_0051379	0.0471	20.8	1	0.0	59	Bln2	
smooth muscle cell differentiation	GO_0011128	0.0487	20.1	1	0.0	61	Cep83	
membrane docking	GO_0022406	0.0487	20.1	1	0.0	61	Bln2	

Table
B14

Appendix Table S4 Primary and secondary antibodies used for immunohistological analysis

Antibody	Provider	Catalog Nr	Dilution
<u>Primary antibody:</u>			
anti AhR rabbit polyclonal IgG	US Bio	031714.200	1:300
anti CD11b rat monoclonal IgG _{2b}	BIORAD	MCA74GA	1:250
anti CD31 rat monoclonal IgG _{2b}	BD Biosciences	550274	1:100
anti CD45 rat monoclonal IgG _{2b}	BD Biosciences	550539	1:500
anti Collagen Type I rabbit polyclonal IgG	Rockland	600-401-103-0.5	1:200
anti Collagen Type IV rabbit polyclonal IgG	Millipore	AB8201	1:40
anti CSPG (CS-56) mouse monoclonal IgM	Abcam	ab11570	1:250
anti GFAP mouse monoclonal IgG ₁ rabbit polyclonal IgG	Sigma Aldrich Dako	G3893 Z0334	1:500 1:500
anti Iba1 rabbit polyclonal IgG	Wako	019-19741	1:500
anti Ki67 rat monoclonal IgG _{2a} rabbit monoclonal IgG	eBioscience Thermo Fisher Scientific	14-5698-82 MA5-14520	1:300 1:100
anti NG2 (CSPG4) rabbit polyclonal	Millipore	AB5320	1:400
anti NeuN mouse monoclonal IgG ₁	Millipore	MAB377	1:100
anti RFP rabbit polyclonal IgG	Rockland	600-401-379	1:500
anti S100(β-Subunit) mouse monoclonal IgG ₁	Sigma Aldrich	S2532	1:250
anti TMEM119 rabbit monoclonal IgG	Abcam	ab209064	1:200
<u>Secondary antibody:</u>			
anti-mouse IgG ₁ Alexa Fluor 488	Thermo Fisher Scientific	A-21121	1:500
anti-mouse IgM Alexa Fluor 488	Thermo Fisher Scientific	A-21042	1:500
anti-rabbit IgG Alexa Fluor 488	Thermo Fisher Scientific	A-21206	1:500
anti-rabbit IgG Alexa Fluor 647	Thermo Fisher Scientific	A-31573	1:500
anti-rat IgG Alexa Fluor 647	Thermo Fisher Scientific	A-21247	1:500
anti-mouse IgG CY3	Dianova	115-165-166	1:500
anti-rabbit IgG CY3	Dianova	111-165-144	1:500
anti-rat IgG CY3	Dianova	112-165-167	1:500